2008

Non-Equilibrium Flow Modeling Using High-Order Schemes for the Boltzmann Model Equations

S Chigullapalli
Purdue University

A Venkattraman
Purdue University

Alina A. Alexeenko
Purdue University - Main Campus, alexeenk@purdue.edu

M S. Ivanov
Khristianovich Institute of Theoretical and Applied Mechanics

40th Thermophysics Conference
23 - 26 June 2008, Seattle, Washington

AIAA 2008-3929

40th Thermophysics Conference, 23-26 June 2008, Seattle, Washington

Non-Equilibrium Flow Modeling Using High-Order Schemes for the Boltzmann Model Equations

S. Chigullapalli*, A. Venkattraman*, and A.A. Alexeenko†

School of Aeronautics & Astronautics, Purdue University, West Lafayette, IN 47907

M.S. Ivanov‡

Khristianovich Institute of Theoretical and Applied Mechanics, Novosibirsk, Russia 630090

We consider application of higher-order schemes to the Boltzmann model equations with a goal to develop a deterministic computational approach that is accurate and efficient for simulating flows involving a wide range of Knudsen numbers. The kinetic equations are solved for two non-equilibrium flow problems, namely, the structure of a normal shock wave and an unsteady two-dimensional shock tube. The numerical method comprises the discrete velocity method in the velocity space and the finite volume discretization in physical space with different numerical flux schemes: the first-order, the second-order minmod flux limiter as well as a third-order WENO scheme. The normal shock wave solutions using BGK and ES collision models are compared to the DSMC simulations. The solution for unsteady shock tube is compared to the Navier-Stokes simulations at low Knudsen numbers and the rarefaction effects in such flow are also discussed. It is observed that a higher-order flux scheme provides a better convergence rate and, hence, reduces the computational effort. The entropy generation rate is shown to be a very sensitive indicator of the onset of non-equilibrium as well as accuracy of a numerical scheme and consistency of boundary conditions in both flow problems.

I. Introduction

In regions of non-equilibrium, which are encountered frequently in supersonic flows at high altitudes and flows expanding into vacuum, the macroscopic conservation laws based on the continuum hypothesis tend to breakdown. The limits on the conventional mathematical models can be understood in terms of the Knudsen number ($Kn = \frac{\lambda}{L}$) where λ is the average distance traveled by the molecules between collisions, or mean free path, and L is the characteristic length scale. When the flow gradients are large, the scale length is of the same order as the mean free path and the transport terms in continuum equations fail. When the continuum equations break down, as in the case of a flow within a normal shock wave and many other flow conditions, a model at the molecular level is required. One approach is to directly simulate the random motion of particles using the Direct Simulation Monte Carlo (DSMC). However, the DSMC method, which allows for non-equilibrium physics, requires high computation power. The mathematical model which describes the motion of molecules is the Boltzmann equation. However, due to it's complex non-linearity, obtaining an analytical solution is not possible for non-trivial problems. Moreover, it presents numerous difficulties to conventional numerical methods. A one dimensional flow of a monatomic gas becomes a four-dimensional problem in phase space with one spatial dimension and three velocity components. Similarly, a two dimensional flow becomes a five-dimensional problem. As a result, it is of great interest

*Graduate Student, Student Member.

†Assistant Professor, AIAA Member.

‡Professor, Head of Computational Aerodynamics Lab, AIAA Associate Fellow.

to apply model equations which are easier to handle than the Boltzmann equation but which also satisfy some of the important properties of the Boltzmann equation viz conservation of mass, momentum and energy.

The model kinetic equations have a long history of application to rarefied gas dynamics problems dating back to 1960s.[1] There is a renewed interest in model equations at present time due to the increased computing power and development of efficient numerical methods for solution of partial differential equations. The main goals of this paper are the investigation and application of different numerical schemes to Boltzmann model kinetic equations to come up with a finite volume numerical method that is both accurate as well as efficient to solve problems involving regions of non-equilibrium. Additionally, we investigate the use of entropy generation rate as an indicator of both onset of non-equilibrium and of numerical accuracy of solution of kinetic equations. The entropy generation rate is considered to be one of the fundamental and most important parameters to predict the onset of non-equilibrium.[2] Thermodynamic equilibrium is characterized by zero entropy generation, and non-equilibrium can be identified by positive entropy generation. That is, a system progresses from one state of thermodynamic equilibrium to a new state of thermodynamic equilibrium through the generation of entropy. Therefore, a single parameter, entropy generation, is identified with thermodynamic non-equilibrium and therefore includes all of the physics which will cause the continuum equations to break down.

We consider various flux schemes for the BGK and the ES-BGK model kinetic equations with collision models. The gradients of the flow properties such as temperature, density, velocity, are extremely steep within a normal shock wave as a result of which the characteristic length scale becomes very small thereby leading to the failure of the continuum equations. Thus, we present the results obtained for the structure of a normal shock wave and 2D viscous shock tube.

II. Kinetic Models

One of the model equations which is widely used is the Bhatnagar-Gross-Krook (BGK) equation.[3,4] The BGK equation with its relaxation type collision term is easier to solve though the number of dimensions in the phase space remain the same as in the Boltzmann equation. It also satisfies the H-theorem (which states that the production of entropy is always positive) and gives a Maxwellian phase density at equilibrium. The phase density $f(x_i, t, c_i)$ is governed by the Boltzmann's equation,

$$\frac{\partial f}{\partial t} + \vec{c}.\frac{\partial f}{\partial \vec{x}} = S \tag{1}$$

II.A. BGK Model

The BGK collision term reads $S_\gamma = -\nu(f - f_\gamma)$ where f_γ is a Gaussian, $f_\gamma = a\,\exp(-\Gamma C^2 + \gamma_i C_i)$, and ν is the collision frequency, $\nu = \frac{p}{\mu}$.

In two dimensions,

$$\frac{\partial f}{\partial t} + c_x\frac{\partial f}{\partial x} + c_y\frac{\partial f}{\partial y} = -\nu(f - f_\gamma)$$

II.B. ES-BGK Model

Another collision relaxation model is the ellipsoidal-statistical model (ES-BGK)[5] where the Maxwellian f_γ of the standard BGK model is replaced by an anisotropic Gaussian and the collision frequency involves the Prandtl number as a parameter. So, the collision term reads $S = -\nu(f - f_G)$. While measurements and the theory of the full Boltzmann equation give $Pr = \frac{2}{3}$ for monatomic gases, one obtains $Pr = 1$ from the standard BGK model. However, the ES-BGK model can reproduce transport coefficients corresponding to arbitrary Prandtl numbers with f_G in the form of anisotropic Gaussian distribution:

$$f_G = \frac{\rho}{\sqrt{det(2\pi\mathbb{T})}}\, e^{\left[-\frac{1}{2}(\vec{c}-\vec{u})^T\mathbb{T}^{-1}(\vec{c}-\vec{u})\right]} \tag{2}$$

where,

$$\begin{aligned}\vec{c}-\vec{u} &= [c_x-u, c_y-v, c_z-w]\\ \rho\mathbb{T} &= \frac{1}{Pr}\rho RTI + (1-\frac{1}{Pr})\rho\ominus\\ \rho\ominus &= <(\vec{c}-\vec{u})\otimes(\vec{c}-\vec{u})f>\\ \rho RTI &= <(\vec{c}-\vec{u})\otimes(\vec{c}-\vec{u})f_\gamma>\end{aligned}$$

For a one-dimensional case, $\mathbb{T}_{11}, \mathbb{T}_{22}$ and $\mathbb{T}_{33}$ are the only non-zero quantities.

Another advantage of the kinetic equations is that these can be coupled with other deterministic solvers, for example, Euler and Navier-Stokes for fluid as well as heat transfer and structural dynamics.

III. Numerical Method

The numerical method is presented in two spatial dimensions, but three dimensions in microscopic velocity. The governing kinetic equation is

$$\frac{\partial f}{\partial t} + c_x\frac{\partial f}{\partial x} + c_y\frac{\partial f}{\partial y} = -\nu(f-f_\gamma) \tag{3}$$

For the numerical solution of the system it is convenient to non-dimensionalize the variables. Each dimensionless quantity is referred to its upstream values at infinity ($\rho_0=\rho_\infty, T_0=T_\infty$), the reference speed $u_0=\sqrt{2RT_\infty}$ and the reference time $t_0=\frac{L}{u_0}$. The reference value for the distribution function is $\frac{n_0}{c_0^3}$.

The space variable is discretized on a Cartesian grid defined by nodes x_{i_1},y_{i_2}. The velocity c_x is discretized using the conventional discrete ordinate method with uniform velocity abscissas $\tilde{c}_x(j_1)=\tilde{c}_{x,min}+(j_1-1)\Delta\tilde{c}_x$ where $\Delta\tilde{c}_x=\frac{(\tilde{c}_{xmax}-\tilde{c}_{xmin})}{N_1-1}$. The velocities c_y and c_z are discretized in a similar manner. A discrete velocity $(\tilde{c}_x(j_1),\tilde{c}_y(j_2),\tilde{c}_z(j_3))$ of the grid will be denoted by $\tilde{c}_j$, where $j=(j_1,j_2,j_3)$ with j_1,j_2,j_3 having a maximum of N_1, N_2 and N_3 respectively. Finally, we also chose a time discretization with $\tilde{t}=n\Delta\tilde{t}$. Thus, the size of the phase space is $N\times N_1\times N_2\times N_3$.

Upon approximation by Finite Volume Scheme the BGK equation is transformed to the system of equations in a 1-D case:

$$f^{n+1} = f^n - \frac{\Delta t}{\Delta x}[F_{i+\frac{1}{2}}-F_{i-\frac{1}{2}}] - \Delta t\nu(f-f_\gamma) \tag{4}$$

For a two dimensional case, the equation would be:

$$\begin{aligned}f^{n+1}_{i_1,i_2,j} = f^n_{i_1,i_2,j} &- \frac{\Delta t}{\Delta x}[F_{i_1+\frac{1}{2},i_2,j}-F_{i_1-\frac{1}{2},i_2,j}]\\ &- \frac{\Delta t}{\Delta y}[F_{i_1,i_2+\frac{1}{2},j}-F_{i_1,i_2-\frac{1}{2},j}]\\ &- \Delta t\nu(f_{i_1,i_2,j}-f_{\gamma,i_1,i_2,j})\end{aligned} \tag{5}$$

III.A. First-Order and Second-Order Flux Schemes

The second order scheme uses a minmod flux limiter scheme.[6]

$$F_{i_1+\frac{1}{2},i_2,j} = \frac{1}{2}[c_x(f_{i_1+1,i_2,j}+f_{i_1,i_2,j}) - |c_x|(\Delta f_{i_1+\frac{1}{2},i_2,j}-\phi_{i_1+\frac{1}{2}},i_2,j)] \tag{6}$$

where $\Delta f_{i_1+\frac{1}{2},i_2,j} = f_{i_1+1,i_2,j}-f_{i_1,i_2,j}$ and

$$\phi_{i_1+1/2,i_2,j} = \begin{cases} 0 & \textit{first order}\\ minmod(\Delta f^n_{i_1-\frac{1}{2},i_2,j}, \Delta f^n_{i_1+\frac{1}{2},i_2,j}, \Delta f^n_{i_1+\frac{3}{2},i_2,j}) & \textit{second order}\end{cases}$$

Similarly,

$$F_{i_1,i_2+\frac{1}{2},j} = \frac{1}{2}\left[c_y(f_{i_1,i_2+1,j} + f_{i_1,i_2,j}) - |c_y|(\Delta f_{i_1,i_2+\frac{1}{2},j} - \phi_{i_1+\frac{1}{2},i_2,j})\right] \tag{7}$$

The flux is non-dimensionalized as follows.

$$\tilde{F} = \frac{Fu_0^2}{n_0} \tag{8}$$

The minmod function can be stated as:

$$minmod(a,b,c) = \begin{cases} min(a,b,c) & a>0, b>0, c>0 \\ max(a,b,c) & a<0, b<0, c<0 \\ 0 & otherwise \end{cases}$$

III.B. Third-Order Flux Scheme

The third order WENO fluxes were calculated using the formulation by Shu.[7] The third order approximation and weights are calculated at each of the eight Gaussian points and the fluxes are then computed by the Gaussian quadrature rule.

III.C. Runge-Kutta Time Marching Scheme

A simple Total Variation Diminishing (TVD) Runge-Kutta scheme by Shu and Osher[7] was used here. In the following sections, f^n is the functional value at time step n. The operator L refers to $-\frac{1}{\Delta x}[F_{i_1+\frac{1}{2},i_2,j} - F_{i_1-\frac{1}{2},i_2,j}] - \frac{1}{\Delta y}[F_{i_1,i_2+\frac{1}{2},j} - F_{i_1,i_2-\frac{1}{2},j}] - (f - f_\gamma)$

III.C.1. Second Order

$$\begin{aligned} f^{(1)} &= f^n + \Delta t\ L(f^n) \\ f^{n+1} &= \frac{1}{2}f^n + \frac{1}{2}f^{(1)} + \frac{1}{2}\Delta t\ L(f^{(1)}) \end{aligned} \tag{9}$$

III.C.2. Third Order

$$\begin{aligned} f^{(1)} &= f^n + \Delta t\ L(f^n) \\ f^{(2)} &= \frac{3}{4}f^n + \frac{1}{4}f^{(1)} + \frac{1}{4}\Delta t\ L(f^{(1)}) \\ f^{n+1} &= \frac{1}{3}f^n + \frac{2}{3}f^{(2)} + \frac{2}{3}\Delta t\ L(f^{(2)}) \end{aligned} \tag{10}$$

IV. Entropy Generation Rate

The second law of Thermodynamics postulates the existence of a state function called the entropy and describes its properties. The expression of entropy is found in the Boltzmann relation from statistical mechanics: $S = kln\Omega$ where S is the entropy, k is the Boltzmann constant and Ω is the statistical multiplicity of the gas. This quantity represents the total number of ways the energy of the collection of particles can be distributed over the system. In the section that follows, only the translational component of entropy is considered since the calculations correspond to a monatomic gas, Argon.

The expression for translational entropy in terms of the velocity distribution function is (Eq. (37)[8]):

$$S_{tr} = k\int_{-\infty}^{\infty} f(\vec{c})\left[1 - ln\left(\frac{h^3 f(\vec{c})}{m^3}\right)\right]d\vec{c}$$

The entropy density can be computed from the velocity distribution functions as Eq. (11).

$$s_{tr} = \frac{1}{\rho}\left\langle k\left[1 - ln\frac{h^3 f}{m^3}\right]\right\rangle \tag{11}$$

The entropy generation rate based on two different definitions is compared below. Since the formulation of this parameter involves the utilization of only statistical mechanics and kinetic theory, there are no inherent mathematical limitations necessary in its calculation.

Kinetic Theory

The first method uses the velocity distribution functions and is obtained from the Boltzmann transport equation. The final expression[8] for the entropy generation rate is given by Eq. (12).

$$\dot{S} = \frac{\partial \rho s}{\partial t} + \nabla . \left(k \int_{-\infty}^{\infty} \vec{c} f(\vec{c}) \left[1 - ln \left(\frac{h^3 f(\vec{c})}{m^3} \right) \right] d\vec{c} \right) \tag{12}$$

Gas Dynamic

An expression for entropy generation rate as a function of macroparameters only can be obtained for small deviations from local equilibrium.[9] For a two-dimensional flow of a monatomic gas, the gas dynamic expression for entropy generation rate is

$$\dot{S} = \frac{\Phi}{T} + \frac{\kappa}{T^2} (\nabla T \cdot \nabla T) \tag{13}$$

where $\kappa = \frac{1}{Pr} \mu C_p = \frac{\mu}{Pr} \frac{\gamma R}{\gamma - 1}$ and Φ is the viscous dissipation function.

Schrock *et. al*[8] have shown that the increase in entropy production entering the shock is predicted later by the Navier-Stokes equations than by DSMC, showing evidence that breakdown parameters based upon continuum data may fail to capture the initial non-equilibrium effects. Their results also show that at lower Mach numbers, the entropy production spike is of the order of the scatter in the DSMC data, which somewhat shows the ability of this parameter to characterize non-equilibrium onset.

V. Results and Discussion

The density, temperature and velocity profiles within the normal shock wave are obtained using first, second, and third order approximations for the fluxes and the solution is compared with that obtained using the DSMC calculations. Numerical fluxes for first and second order schemes are obtained using the minmod flux limiter.[10] To compute the third order fluxes, we used the Weighted Essentially Non-Oscillatory (WENO) scheme.[7] Total-Variation-Diminishing (TVD) Runge-Kutta[11] type time discretization was used for second and third order accurate solutions in time. The numerical schemes were implemented in FORTRAN 90 and MPI was used for the parallel version of the code.

Normal Shock Wave

The results presented below were computed for a normal shock wave in Argon gas at a Mach number of M=1.4 with boundary conditions as shown in Table 1. The results shown in Fig. 1 correspond to a grid of 51 points. For the first order flux scheme, we used a non dimensionalized time-step of 10^{-4} for first order accuracy in time. Similarly, computations involving second and third order fluxes were accurate up to second order and third order in time respectively. For the second order and third order TVD Runge-Kutta schemes, time-steps of 2×10^{-4} and 5×10^{-4} were used respectively. All the variables were non-dimensionalized by the corresponding upstream values. The reference speed is $c_\infty = \sqrt{2RT_\infty}$ and reference time is L/c_∞ where L is the length of the domain (45λ for a Mach number, $M = 1.4$). When L_2 norm of the change in density and temperature with each time-step is less than 10^{-6}, the steady state solution was assumed to have been reached. It has been observed that the WENO third order scheme requires less CPU time and number of iterations than the other schemes for convergence as shown in Table 2.

The DSMC simulation used 300 cells and a total of about 19,400 molecules. The number density was 10^{20} and each simulated molecule represented 0.4×10^{16} real molecules. The average number of molecules per cell was 50 and 80 for cells upstream and downstream of the shock respectively. A total of 8.74×10^4 iterations with a time step of 0.75×10^{-6} were needed to reach steady state. The macro-parameters were sampled over another 58,000 time steps. The simulation using the Fortran code DSMC1S.FOR by G. A. Bird[12] took a total time of 10 hours on one processor. The BGK solver took more than 24 hours for convergence using

Table 1. Conditions across a Normal Shock of Mach number $M = 1.4$

Property	Upstream	Downstream
Density	1.0	1.581
Velocity	1.278	0.808
Temperature	1.0	1.392
Pressure	1.0	2.2

Table 2. Comparison of number of iterations to convergence and CPU times for different flux schemes

Scheme	No. of iterations	CPU time(hr)
First Order Flux	115500	24
Second Order Flux	340000	14
WENO Third Order Flux	130000	8

first order scheme, 14 hours with the second order scheme and 8 hours with the third order scheme.

The comparison between density and temperature profiles obtained using different flux schemes and DSMC for the case of $M = 1.4$ is shown in figures 1(a) and 1(b). The shock thickness from the simulations using the third order flux scheme agrees well with DSMC simulations. Figure 2 shows the comparison of density and temperature profiles obtained using the BGK, ES-BGK model, both using WENO flux scheme, and DSMC. It can be seen that the results obtained using the ES-BGK model agrees extremely well with that obtained using DSMC.

Figure 4 shows the comparison of the entropy generation rate obtained using the gas dynamic definition Eq. 13 and the kinetic theory definition Eq. 12. The entropy generation rate predicted using the WENO third order flux scheme and 200 cells agrees well with the result predicted by the gas dynamic definition. The trend shown by the solution obtained using the first and second order flux schemes do not match well with the expected trend even for a fully converged solution with 800 cells. For fewer grid points, the solution using the first order scheme shows a non-positive entropy generation rate. As the number of cells is increased, the entropy generation using the first order scheme approaches that from the third order scheme. The peak from the first order scheme in Fig. 4(a) is at 120 and it reduces to 52 in Fig. 4(b). Thus the entropy generation rate is an indicator of the convergence of numerical solution in the number of grid points.

Figure 3 shows the specific entropy profile for the normal shock for the three different flux schemes. With 200 grid points, the second and third order schemes give almost the same specific entropy profile but the second order scheme does not predict the entropy generation rate correctly.

Entropy generation rate can also be an indicator of the correct implementation of the boundary conditions as well as the size of the computational domain. For a steady normal shock simulation the macroscopic properties on the left and right boundary are coupled by the Rankine-Hugoniot equations. A numerical error occurs due to the discretization of the velocity and re-calculation of macro-properties from the discretized values. Now, these new values of the macroscopic properties do not satisfy the normal shock relations exactly and this shows up as oscillations in the entropy generation rate at the boundaries as shown in Figure 5(a). However, it does not show up in the density, temperature and specificentropy profiles. Figure 5(b) shows a comparison of the density profiles obtained using conservative and non-conservative boundary conditions. The correct implementation of boundary conditions would be to solve the system of equations (mass, momentum and energy conservation) for the equilibrium distribution function that recovers the macroscopic properties exactly.

Figure 6 shows the normalized density and entropy generation rate profiles for an upstream Mach number 3.0. The results presented, compare the profiles obtained using both the BGK and the ES-BGK collision models. Clearly, the BGK model predicts a steeper shock profile when compared to the ES model. Compar-

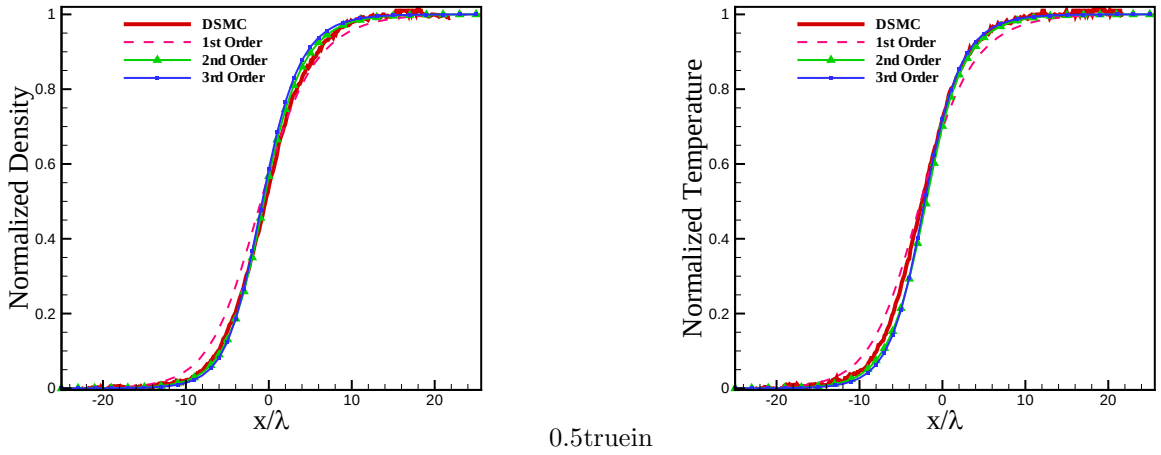

(a) Density profile. (b) Temperature profile.

0.5truein

Figure 1. Normal Shock Structure, $M = 1.4$

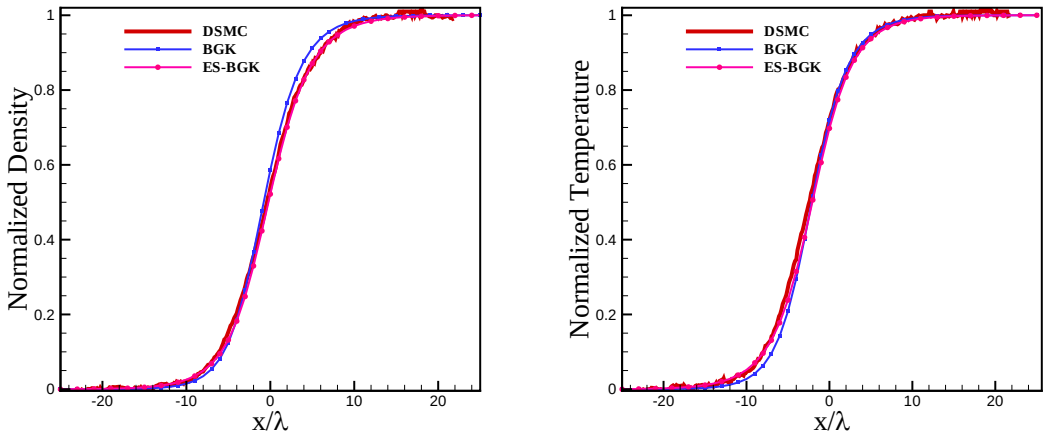

(a) Density profile. (b) Temperature profile.

Figure 2. Normal Shock Structure, $M = 1.4$**, Comparison of ES-BGK, BGK model with DSMC**

isons between the entropy generation rates obtained using the gas dynamic and the kinetic theory expressions indicate that, for a strong shock, the gas dynamic expression based only on the macro parameters fails to predict accurately, the region of non-equilibrium upstream of the shock. This shows that, though the macro parameters are calculatedbased on a molecular approach, the gas dynamic expression is insufficient to fully describe the non-equilibrium regions in the flow field.

One of the important properties of a shock wave in a monatomic gas is the temperature overshoot.[13] From the conservation equations, it can be shown that, T_x is related to the number density n as follows

$$\frac{T_x}{T_1} = \frac{1}{3}\left[(5M_1^2+3)\frac{n_1}{n} - 5M_1^2\left(\frac{n_1}{n}\right)^2\right] \tag{14}$$

From the above expression, it can be shown that T_x possesses a maximum for all shocks if M_1^2 is greater than 9/5. The analytical profile of the temperature associated with the longitudinal thermal velocities, T_x, can be used to compare the accuracy of the solutions obtained using different flux schemes. We present results for the variation of $(T_x - T_1)/(T_2 - T_1)$ as a function of $(n - n_1)/(n_2 - n_1)$ for $M_1 = 2$. Though there

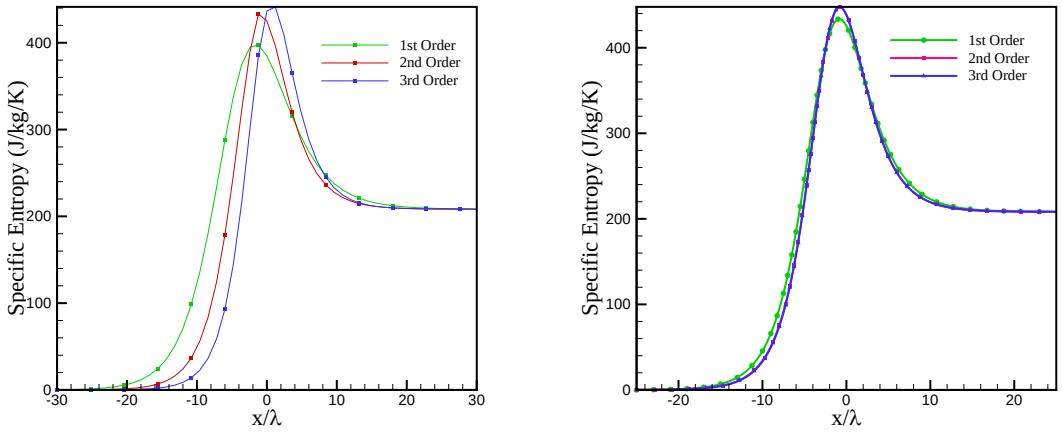

(a) 51 grid points (b) 201 grid points

Figure 3. Entropy profile for Mach number, $M = 1.4$

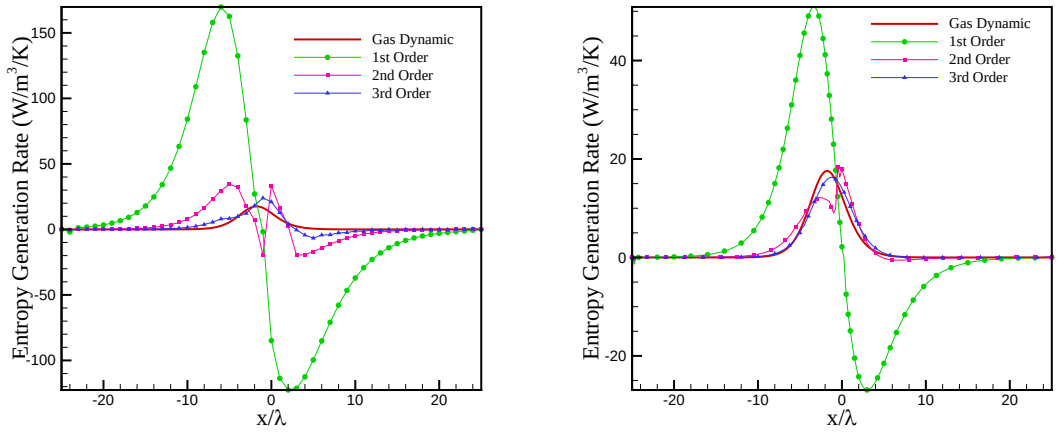

(a) 51 grid points. (b) 201 grid points.

Figure 4. Normal Shock. Entropy Generation profile, $M = 1.4$

is an overshoot in T_x for all values of $M > 1.34$, the amount of overshoot is quite small for $M = 1.4$ and hence results are presented for cases which show the overshoot clearly. Results (Figure 7(a)) are also shown for the case of $M = 2$, to compare the results obtained using the second order flux scheme and the third order WENO scheme for a grid with 51 points. For this case, the solution is not fully converged but a case which provides a clear picture of the differences between the solution obtained using the two Flux schemes). Figure 7(b) shows a comparison of the variation of T_x and indicates that the result obtained by using 401 grid points with the second order flux scheme can be reproduced with a lesser number of grid points using the third order WENO scheme and both solutions match well with theory.

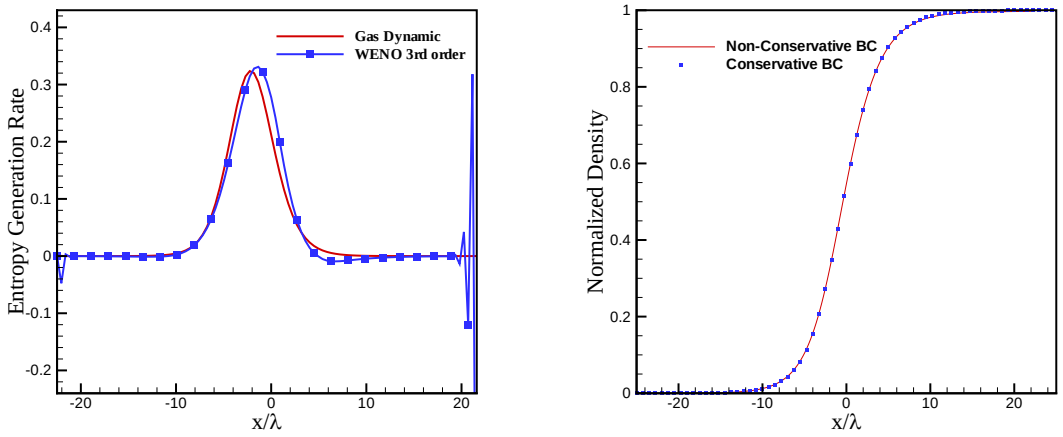

(a) Entropy generation profile (b) Density profile

Figure 5. Non-conservative boundary conditions

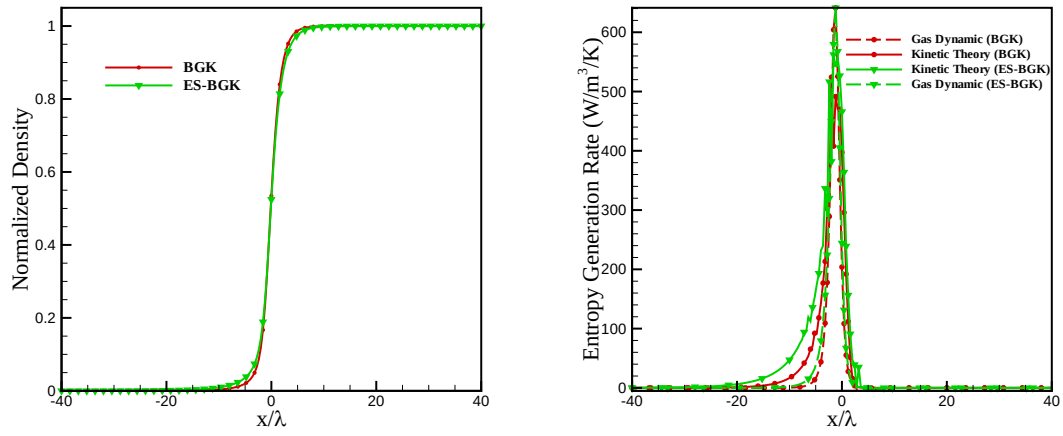

(a) Normalized density (b) Entropy generation rate

Figure 6. Normal Shock. Normalized density and entropy generation rate profiles, $M = 3.0$

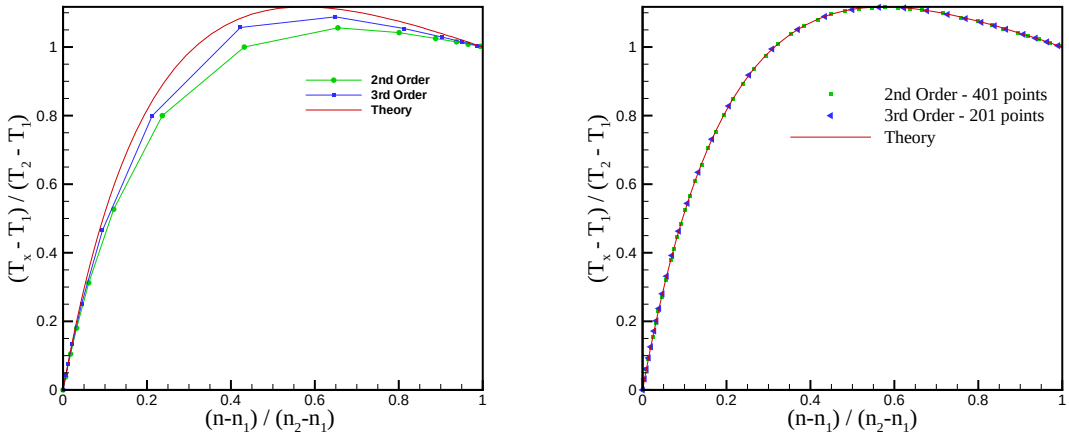

(a) 51 grid points

(b) 2nd order scheme - 401 grid points and 3rd order scheme - 201 points

Figure 7. Comparison of T_x profiles for a normal shock, $M = 2$

V.A. 2D Shock-Tube Problem

A well-known one-dimensional flow problem is the Riemann problem,[14] which treats the development of a flow due to an initially discontinuity. Removing the membrane separating the gas in the two reservoirs, results in a characteristic wave pattern consisting, in general, of three waves, a shock wave, an expansion fan, and a contact discontinuity and the inviscid shock-tube problem can be solved exactly using gas-dynamic theory. In commonly used shock-tubes in laboratories, the boundary layer effects are negligible and the problem can be considered one-dimensional for all practical purposes. However, to get high Mach numbers, the initial pressure ratio is extremely high and this increase the burden on vacuum pumps. In case a desktop shock tube were used, it is easier and faster to pump down the chambers to get the high pressure ratios due to their smaller dimensions. But at the micro-scales[15] the boundary layer effects are not negligible. Shock tubes are also used to induce faster combustion and their use in micro devices is an active area of research.[16,17] Here, we present results for the simulation of two cases with Knudsen numbers(Kn) in the range 0.01-1 using the model equation and compare the lower Knudsen number case with compressible Navier-Stokes simulations using FLUENT.

The diaphragm in the shock tube is located at $x = L/2$ where L is the length of the domain and h is the height. The Argon gas to the left of the interface is at a pressure of $10Pa$ and temperature $300K$. This corresponds to a density of 1.603×10^{-4} kg/m^3. The pressure on the right of the interface is set to 1Pa and temperature is set to 300K. In the non-dimensional form, these values are shown in Table 3. The length and height of the channel were 1 m and 0.05 m respectively. This gives Knudsen numbers of 0.01 and 0.1 in the high and low pressure sections respectively. The dimension of the phase space in the Kinetic WENO solver is taken to be $160 \times 80 \times 20 \times 20 \times 20$. For the FLUENT simulation, a 300×100 mesh was used with a non-uniform grid in the y-direction with a successive ratio of 1.2. Figures 8-10 show the temperature, pressure, velocity, entropy, and entropy generation rate (based on gas dynamic expression) contours for both FLUENT and kinetic solutions at time $\widehat{t} = 2.12$ where $\widehat{t} = 1$ implies the theoretical time it takes for a shock to move a distance equal to h. It can be seen that the shock is more attenuated in the FLUENT simulation than in the BGK solution. This is due to the slip effects that are accounted for in the kinetic equation but not in the Navier-Stokes simulation. In regions close to the line of symmetry, the contours of entropy generation rate show three peaks corresponding to three different regions of non-equilibrium, the compression wave, the contact discontinuity, and the rarefaction wave. At the walls of the shock tube, the interactions between the boundary layer and the wave system, lead to more complicated contours.

A second case was run with the same grid resolution and pressure ratio but a different initial pressure as shown in Table 4. The Knudsen number in the left zone is 0.1 and in the right zone is 1.0. Case 2 gives

Table 3. 2D Shock-tube: Initial conditions to the left and right of interface.

Property	Left Zone	Right Zone
Density	1.0	0.1
x-velocity	0	0
y-velocity	0	0
Temperature	1.0	1.0
Pressure	1.0	0.1

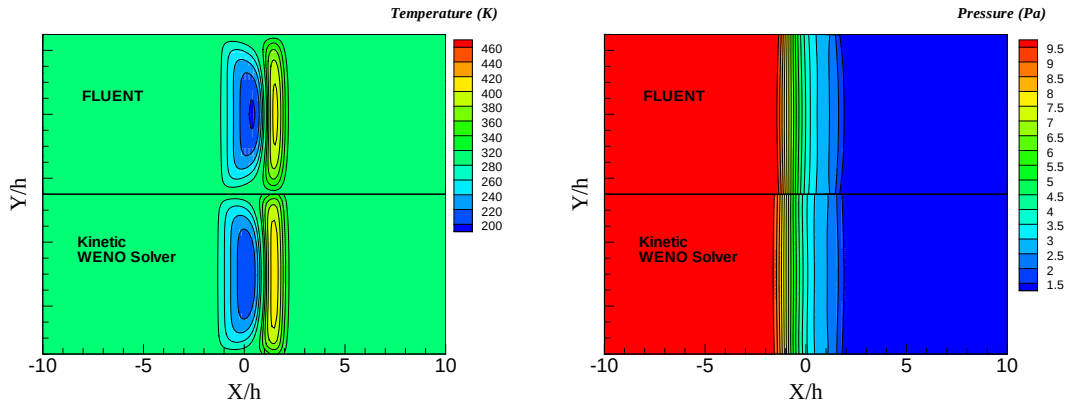

Figure 8. 2D shock-tube: Static pressure and temperature contours for $Kn = 0.01 - 0.1$ at $\widehat{t} = 2.12$.

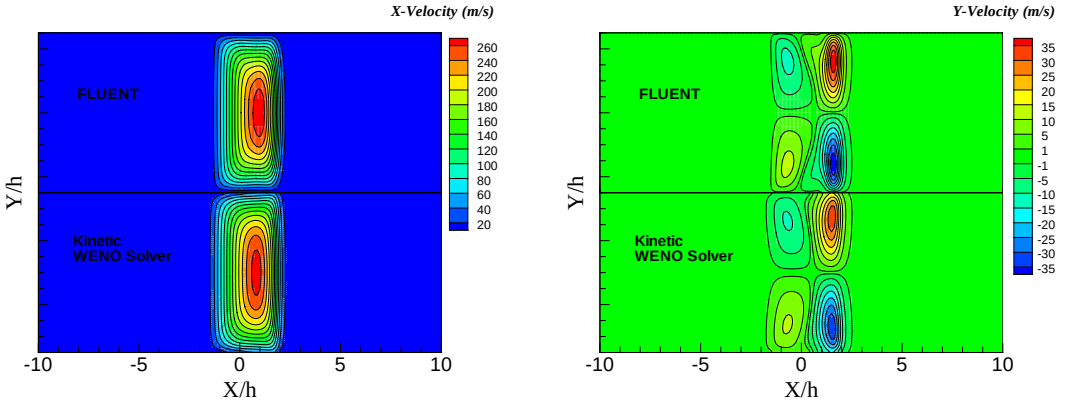

Figure 9. 2D shock-tube: Velocity contours $Kn = 0.01 - 0.1$ at $\widehat{t} = 2.12$

profiles very different from Case 1 that are the manifestation of rarefaction effects. Figure 11 shows the static temperature and x-velocity profiles from the kinetic solver for both these cases at time $\widehat{t} = 3.53$. It can be seen from these profiles that the shock wave is slowed down more in Case 2 than in Case 1 when compared to the theoretical position of $x = 3.53h$ based on inviscid theory.[14]

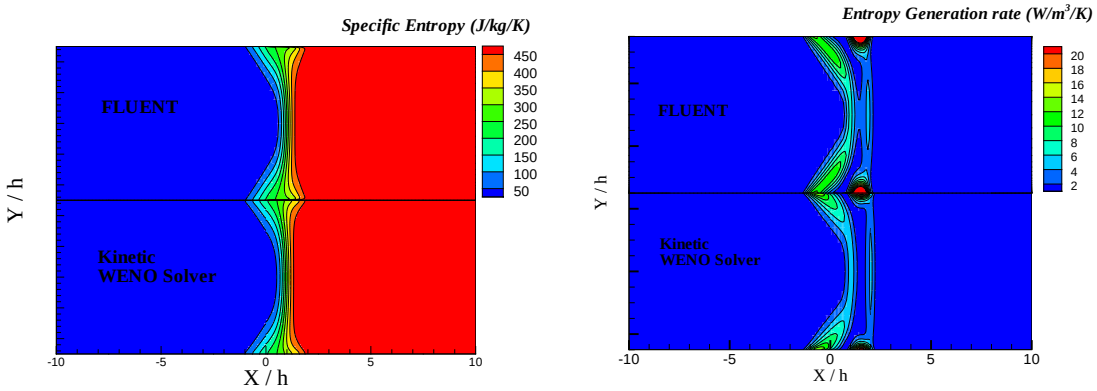

Figure 10. 2D shock-tube: Entropy and Entropy generation rate contours $Kn = 0.01 - 0.1$ **at** $\widehat{t} = 2.12$

Table 4. Initial conditions for the different cases

Property	Case 1	Case 2
ρ_0	$1.604E-4\text{kg}/m^3$	$1.604E-5\ \text{kg}/m^3$
T_0	300K	300K
P_0	10Pa	1Pa

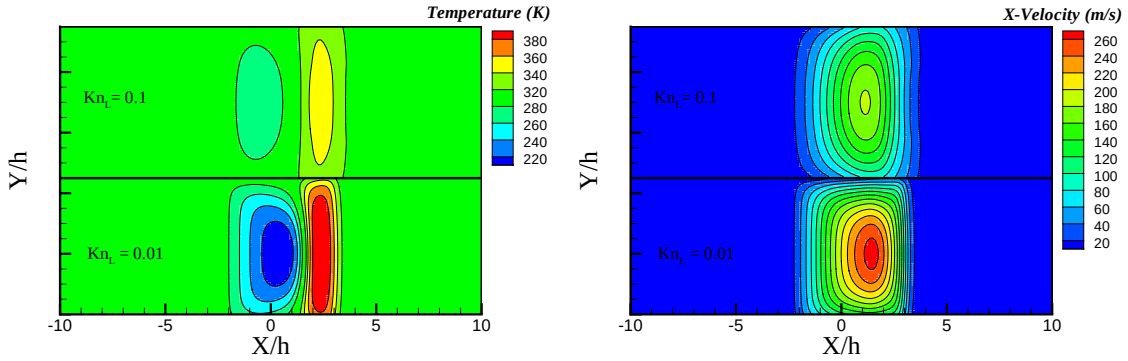

Figure 11. 2D shock-tube: Static temperature and x-velocity profiles for the 2 cases at $\widehat{t} = 3.53$.

VI. Conclusions

High-order methods can provide accurate solution of kinetic model equations and significantly decrease computational cost. The density and temperature profiles across a normal shock wave calculated using the ES-BGK model compared well with those obtained from DSMC. Entropy generation rate can be used as an indicator of accuracy of the numerical solution and the onset of non-equilibrium. At lower Mach numbers for a normal shock, the entropy generation rate based on the two expressions, gas dynamic and kinetic theory, match well and at higher Mach numbers the gas dynamic expression gives a conservative estimate. At Mach number 3, the width of the non-equilibrium zone based on the gas dynamic expression of entropy generation rate is much smaller than that based on the kinetic theory expression.

The solver was verified by comparison with DSMC solutions for the test cases of a normal shock. It should be mentioned that our solver is perfectly conservative for density, momentum and total energy. The entropy is increasing across a normal shock wave as predicted by the Boltzmann's H-Theorem. It has also been shown that the entropy generation rate can be an indicator of the quality of the numerical solution. The solver was also used to solve an unsteady viscous shock tube problem in the slip regime and the solution compared with the Navier Stokes solution obtained using FLUENT. Based on this investigation, we aim to come up with a highly efficient solver that can be used to solve other complex non-equilibrium flows.

VII. Acknowledgments

The computations reported in this paper were performed on 16 CPU Sunfire 4600 awarded through Sun Microsystems, Inc. Academic Excellence Grant #EDUD-7824-070336-US.

References

[1]Cercignani, C., *The Boltzmann Equation and Its Applications*, Springer, 1988.

[2]Schrock, C. R., McMullan, R. J., and Camberos, J. A., "Calculation of Entropy Generation Rates via DSMC with Application to Continuum/Equilibrium Onset," *38th AIAA Thermophysics Conference*, AIAA, Toronto,Ontario,Canada, 2005.

[3]Bhatnagar, P. L., Gross, E. P., and Krook, M., "A model for collision processes in gases. I. Small amplitude processes in charged and neutral one component systems," *Physical Review*, Vol. 94, 1954, pp. 511.

[4]Krook, M., "Continuum equations in the dynamics of rarefied gases," *Journal of Fluid Mechanics*, Vol. 6, 1959, pp. 523.

[5]Holway, L. H., "New statistical models for kinetic theory: Methods of construction," *Physics of Fluids*, Vol. 9, 1966, pp. 1658.

[6]Harten, A. and Osher, S., "Uniformly high-order accurate non-oscillatory schemes," *SIAM Journal of Numerical Analysis*, Vol. 24, 1987, pp. 279–309.

[7]Zhou, T., Li, Y., and Shu, C.-W., "Numerical Comparison of WENO Finite Volume and Runge-Kutta Discontinuos Galerkin Methods," *Journal of Scientific Computing*, Vol. 16, No. 2, 2001, pp. 145–177.

[8]Schrock, C. R., McMullan, R. J., and Camberos, J. A., "Continuum Onset Parameter Based on Entropy Gradients Using Boltzmann's H-Theorem," *43rd AIAA Aerospace Sciences Meeting and Exhibit*, AIAA, Reno,Nevada, 2005.

[9]Naterer, G. F. and Camberos, J. A., "Entropy and the Second Law Fluid Flow and Heat Transfer Simulation," *Journal of Thermophysics and Heat Transfer*, Vol. 17, No. 3, 2003, pp. 360–371.

[10]Mieussens, L. and Struchtrup, H., "Numerical comparison of Bhatnagar-Gross-Krook models with proper Prandtl number," *Physics of Fluids*, Vol. 16, No. 8, 2004, pp. 2797–2813.

[11]Shu, C.-W. and Osher, S., "Efficient Implementation of Essentially Non-oscillatory Shock-Capturing Schemes," *Journal of Computational Physics*, Vol. 77, 1988, pp. 439–471.

[12]Bird, G. A., *Molecular Gas Dynamics and the Direct Simulation of Gas Flows*, Oxford University Press, New York, 2nd ed., 1994.

[13]Yen, S.-M., "Temperature overshoot in shock waves," *Physics of Fluids*, Vol. 9, No. 7, 1966, pp. 1417–1418.

[14]Schreier, S., *Compressible Flow*, Wiley, New York, 2nd ed., 1982.

[15]Iancu, F. and Muller, N., "Efficiency of Shock Wave Compression in a Microchannel," *Microfluid Nanofluid*, Vol. 2, 2006, pp. 50–63.

[16]Brouillette, M., "Shock Waves at Microscales," *Shock Waves*, Vol. 13, 2003, pp. 3–12.

[17]Zeitoun, D. E., Burtschell, Y., Graur, I. A., Ivanov, M. S., Kudryavtsev, A. N., and Bondar, Y. A., "Shock Waves at Microscales," *West-East High Speed Flow Field Conference*, Moscow,Russia, 2007.